Current Science International
Volume: 15 | Issue: 03| July – Sept.| 2026

EISSN:2706-7920 ISSN: 2077-4435
DOI: 10.36632/csi/2026.15.3.17
Journal homepage: www.curresweb.com
Pages: 217-238

Investigation of Economic Heavy Minerals in East El Gharbia Drainage, North Delta, Egypt

S. M. El Alfi

Nuclear Materials Authority, P.O. Box: 530 El Maadi, Cairo, Egypt.

Received: 20 June 2026 **Accepted:** 10 August 2026 **Published:** 30 August 2026

ABSTRACT

The study area extend from East El Gharbia drainage from the West to new El Mansoura city from the East with total length of about 18km, while the width extend from the beach southward to the International High way ranging from 0.750km to 1.60km with total area of about 24.50km^2. This study is mainly concerned to the muddy coast. The coastal environment is the area lying at the interface between the land and the sea. The area is covered by two profiles oriented parallel to the shoreline with 1 km spacing. About 32 stations were drilled in east El-Gharbia drainage, two-meter depth in every station. The first profile located near and referred by simple (WK), the second profile located southward the first one and near to the International High and referred by simple (WKS), The total samples which collected from the area are 64 samples. The total heavy minerals content in the 1st meter in profile (WK) range from 3.60% to 9.17% with an average of 6.104%, in the 2nd meter in the same profile range from 2.95% to 5.73% with an average of 4.451%. Its content in the 1st meter in profile (WKS) range from 4.61% to 6.83% with an average of 5.622%, in the 2nd meter in the same profile range from 4.30% to 6.86% with an average of 5.61%. The total economic minerals content in the 1st meter in profile (WK) range from 1.01% to 2.59% with an average of 1.62%, in the 2nd meter in the same profile range from 0.88% to 1.77% with an average of 1.39%. Its content in the 1st meter in profile (WKS) range from 1.07% to 1.55% with an average of 1.28%, in the 2nd meter in the same profile range from 0.86% to 1.59% with an average of 1.22%. The identified heavy mineral assemblages studied under a Binocular Stereomicroscope in the studied area can be classified into two main groups according to Folk (1980). The first one includes opaque minerals as; Magnetite, Hematite, Ilmenite, Leucoxene. The second group comprises non-opaque minerals includes Garnet, Zircon, Rutile, Monazite and Titanite. The accessory minerals as: Staurolite, Pyrite, Apatite, Chromite, kyanite.

Keywords: East El Gharbia, drainage, economic heavy minerals, black sand beach

1. Introduction

After foundation the Egyptian black sand company (EBSC) in 2015 by collaboration with Egyptian Nuclear Materials Authority (NMA). Egyptian Nuclear Materials Authority constructed a semi-industrial plan for the exploitation of the black sand sediments at coastal area of Mediterranean Sea. A location map was constructed by NMA which shows 13 main black sand localities on the Mediterranean sea coast (Fig. 1). For the completion and continuation of this plan to investigate and evaluate the economic heavy minerals on industrial scale, the present work is planned to investigate the mineralogy of economic heavy minerals including radioactive minerals for beach and coast sediments, north Delta, Egypt, East El Gharbia drainage.

The heavy minerals in the Mediterranean Sea coast transported by the river Nile from Central Africa through two main sources: the Abyssinian Plateau and the northern Lake Region of the Central African Plateau. The water carries huge amounts of deposits derived from the denudation of all igneous and metamorphic rocks. Most of these deposits are including heavy economic minerals. The rich placer deposits of heavy economic minerals have been deposited along the northern beaches on the delta coast.

Corresponding Author: S. M. El Alfi , Nuclear Materials Authority, P.O. Box: 530 El Maadi, Cairo, Egypt.
E-mail: samehelalfi2@gmail.com

These sediments are pushed towards the beaches and the submerged offshore sandbars by displacement in suspension and saltation. Through this phase of transportation under the seawater in the shelf area, the grains undergo an effective action of sorting. During the transportation of these sediments some mineral grains turn to be polished and free of contaminations while others are entirely lost before reaching the influx. The subsequent wind action transports, some of these sediments accumulated as sand accumulations and sand dunes along the beach (El Kammar *et al*., 2010).

Google earth image (Fig. 2) shows the study area (delineated area) which extend from East El Gharbia drainage from the West to New El Mansoura City from the East with total length of about 18km, while the width extend from the beach southward to the International High way ranging from 0.750km to 1.60km with total area of about 24.50km^2. This area is close to El Burullus sand dunes which is the most potential occurrence of minerals sand, the evaluation of this area is most important where it represent natural extenuation of El Burullus sand dunes. The Nile Delta coast and Nile branches in classical time are shown in figure (3) after Wiegel (2009) which shows the old extinct branch Sebennitic close to the area of study.

The studied area The accessibility of the area is good, the entrance to the area is mainly from the international high way Road. The climate is cold in winter and warm in summer, and the rain falling are highly frequencies and density in winter season. Vegetation is moderate dense, while the habitants have been used the inter-dunes space for cultivation.

In Egypt, the wind speed generally decreases both inland and to the east. The study area is mainly affected by the northwest direction wind coming from the Mediterranean Sea, which sometimes changes to the northeast direction. In addition, the wind speed tend to be low in August, and increased progressively in November to January; it reaches its maximum in April, which created dust storms known as "Khamasin".

These sediments occur along the Mediterranean Sea coast in a zone extending from Abu Qir in the west to El Arish in the east. They occur in two forms, beach deposits and coastal sand dunes. Extensive black sands placer deposits are discontinuously distributed along the northern Mediterranean coastal plain of the Nile Delta as: El-Hadary (1998); El Balakssy (2003); El Azab *et al*. (2018, 2019), Samy and El-Gohary (2013); Ragab *et al*. (2017); Shousha *et al*. (2019); El Alfi (2019); El Alfi *et al*. (2023), El Afandy *et al*. (2016,2022) and Awad *et al*. (2023).

Geomorphology of the studied area.

The northern Egyptian shoreline extends from Rafah at the east to El Salom at the west (Fig. 4). According to El Rakaiby and Attia (2004) the northern coast can be divided into three parts which coasts possess different morphological forms and geological units as follow:

1. The sandy or Sinai coast (eastern coast) extends from Rafah to Romana
2. The muddy or Delta coast (central coast) extends from Romana to El Dikhela.
3. The rocky or the north western desert coast (western coast) extends from El Dikhela to El Salom.

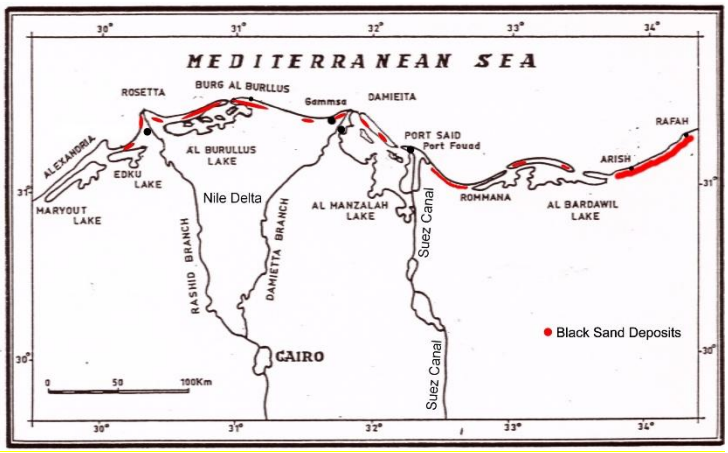


Fig. 1: Nile Delta map showing location of the main black sand deposits (NMA).



Fig. 2: Google earth image showing location of the study area.

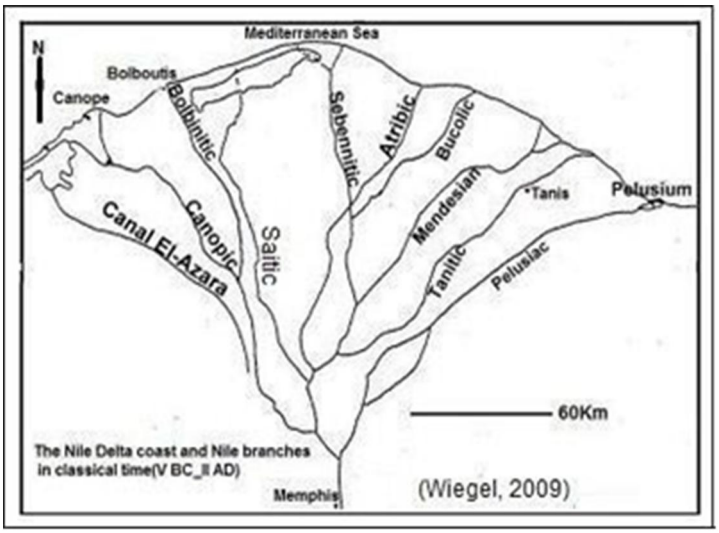


Fig. 3: The Nile Delta coast and Nile branches in classical time (V BC-II AD) (after Wiegel, 2009).

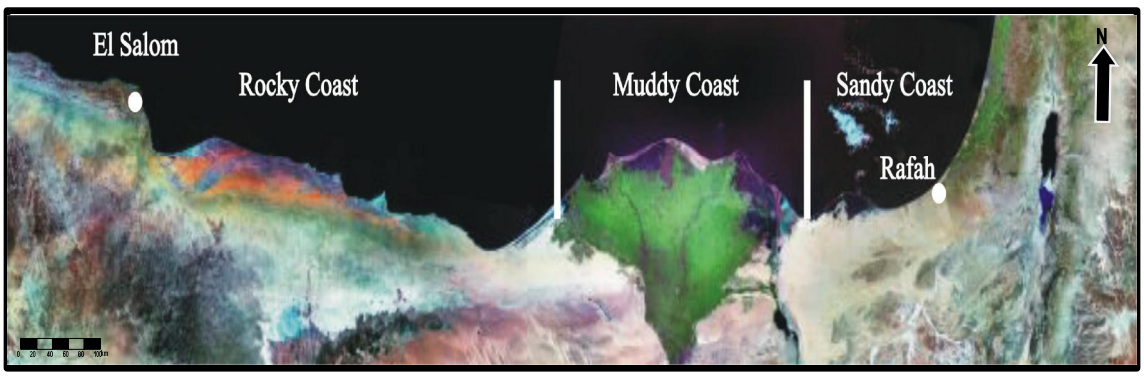


Fig. 4: TM Landsat image band-7 shows the northern Egyptian coast plain.

This study is mainly concerned to the second coastal division (muddy coast). The coastal environment is the area lying at the interface between the land and the sea. As in other geomorphic environments, coastal areas are composed of a wide range of landforms. The coastal environment includes both the zone of shallow water within which waves are able to move sediment, and the area land-ward of this zone, including:- 1) beach areas (shore) and 2) coastal plain. These landforms are affected to some degree by the direct or indirect effects of marine waves, tides and currents.

1) Beach

Beach (Shore), which is the strip of ground bordering any body of water, over with the beach sands actively oscillate with changing wave action.

Water in Mediterranean Sea is in constant motion as the other oceans of the world. It moves by wind generated waves, tides, and a variety of currents. It constantly modifies the shores, reshaping coastlines with less activity of waves and currents. The Delta beaches are composed of unconsolidated and readily transportable sand, occasionally, they can adjust quickly to changes in the nature and energy of coastal processes.

The Holocene has been great changes in the position of shorelines and in coastal morphology as a result of predominantly rising sea levels. Shoreline processes can change in intensity from day to day, and from season to season but they never stop. According to Keller, (2000), winds generated waves period most of the energy for shoreline processes. The refraction waves concentrate energy on headlands (such as Rashid and Dumyat heads). One of the most important shoreline processes is the long-shore drift current which generates by waves advancing obliquely lowland the shore.

In general, the Delta shorelines are especially important because they include economic minerals deposited associated with their beach sands, as well as the concentration of population on/or near the coasts.

The Mediterranean shore in front of the Nile Delta is nearly flat, narrow, and underline fine to very fine sand. As the beginning of 20th century where low floods associated with deficiency in sediment load, the coast was changed from emerged to submerged and the progressive accretion has been changed at several places, into erosion of varying rates.

The study area generally is a flat beach with no cusps. The for-shore is a narrow stretch with gentle slope toward the sea where the beach in this area represents an accretion zone. The shape of the beach in the study area is mainly convex (Fig. 5a) and concave in some parts inside the main convex shape (Fig. 6).

2) Coastal plain

The coastal area, is the land and sea areas bordering the shore line, While the coastal plain is an area of lowland adjacent to the sea, and resulting from the accumulation of marine or alluvial sediments. Where formed by marine sediments the coastal plain has been exposed by a relative fall of sea-level. However, the coastal line is that line forms the boundary between the coast and the shore; commonly forms boundary between land and water.

The coastal plain in the study area is vary in wide ranging from 0.750 to 1.60 km. It used for agriculture, and building of village for fisher and farmers. The studied area is flat free from sand dunes except some scattered sand accumulation near the shore (Fig. 5b&c) and the ripple mark which found in the coastal plain is characteristic features (Fig. 5d &e).

2. Materials and Methods

Sampling

According to the suggested plane, the area is covered by two profiles oriented parallel to the shoreline with 1 km spacing. About 32 stations were drilled in east El-Gharbia drainage using auger equipment for two-meter depth in every station. The first profile located near the shore and include 18 station and drilled to depth 2m so the total samples are 36 and referred by simple (WK). The second profile located southward the first one and near to the International High way road and include 14 station and drilled to depth 2m so the total samples of 28 and referred by simple (WKS), so the total samples which collected from the area are 64 samples from 32 station. These samples are plotted on the Google Earth photo (Fig. 6). Their weight of each collected sample is ranging from 5 to 7 kg. These samples transported to nuclear materials authority laboratory for treatment, and analyses.

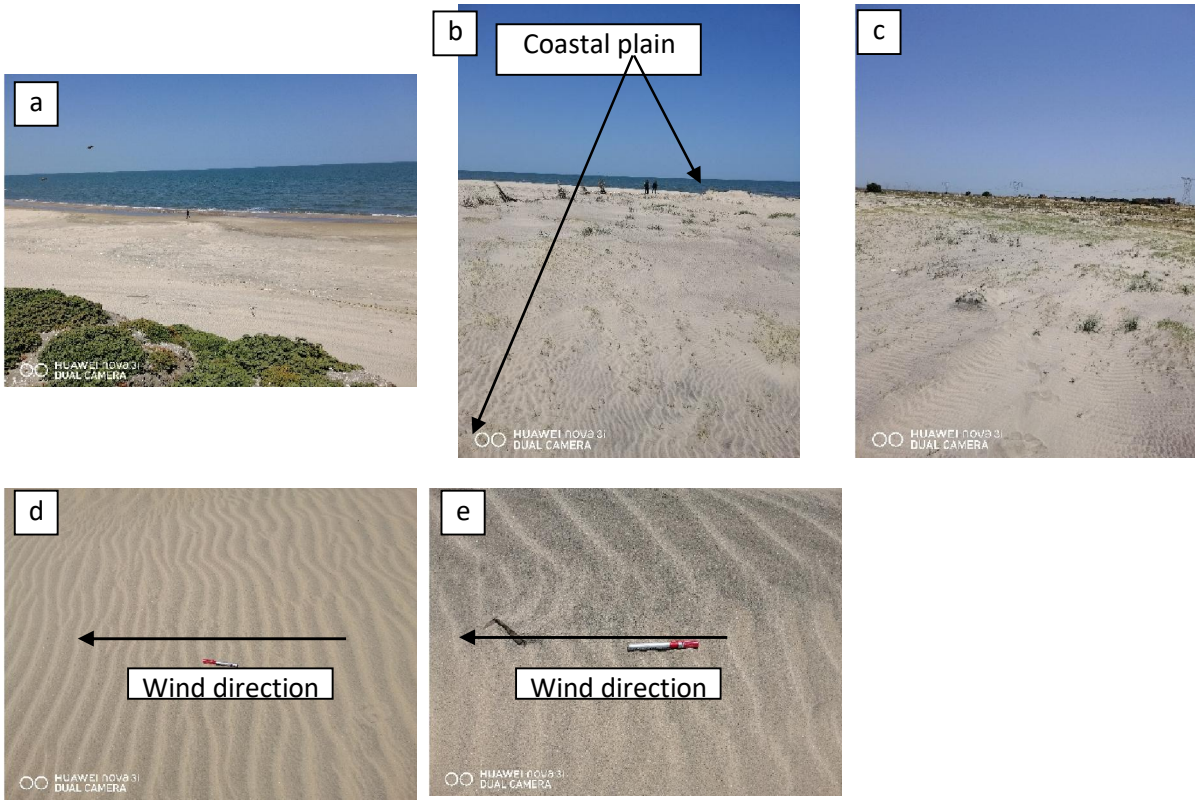


Figure (5): Photograph shows: a) the beach (shore), b& c) coastal plain with some sand accumulations and d& e) the ripple marks in the coastal plain.

Preparation of Samples and Techniques

The original sand samples were dried and passed from sieve 0.8 mm to remove the shell, shell fragments, and the gravel. The sample is quartered by John's splitters of different chutes until about 250gm, the rest sample was saved as reference sample.

A representative sub-sample weighting about 60gm was taken from each prepared sample by quartering for mineral separation. The gravimetric separation is used to separate the heavy minerals from the light minerals by using the heavy liquid bromoform with specific gravity of 2.86 g/cm³. Heavy fractions were dried, weighted and their percentages were calculated and tabulated in Table (1). The light fractions were discarded, while the heavy fraction is used for further analysis. The magnetite separation carried out using a small hand magnet with suitable strength and their percentages calculated and tabulated in Tables (3, 4, 5 and 6) for profile (WK) and profile (WKS).

The free-magnetite samples were subjected to the magnetic separation using Frantz Isodynamic Magnetic Separator (Model L-1) at 0.2, 0.5, 1.0, 1.5 magnetic and 1.5 non-magnetic current amperes. Each fraction obtained from the magnetic separation process was microscopically studied under binocular stereomicroscope and investigated to calculate the percentages of the concerned minerals in the samples. The percentage of each mineral were calculated to the original samples also ranges and averages of the total heavy mineral for the studied sediments and tabulated in Tables (3 & 4) for profile (WK) and Tables (5 & 6) for profile (WKS).

Mineralogical investigation of the mineral constituents was carried out by Semi-quantitative EDX chemical analyses using a Phillips XL-30 Environmental Scanning Electron Microscope (ESEM) on individual grains of heavy minerals.

The identified heavy mineral assemblages studied under a Binocular Stereomicroscope in the studied area can be classified into two main groups according to Folk (1980). The first one includes opaque minerals as; Magnetite, Hematite, Ilmenite, Leucoxene. The second group comprises non-opaque minerals includes Garnet, Zircon, Rutile, Monazite and Titanite. The accessory minerals as: Staurolite, Pyrite, Cassiterite, Apatite, Chromite. The most important heavy minerals will be described in the following paragraphs:

3. Results and Discussion

The distribution of the total heavy minerals between 1st and 2nd meter were graphically represented using lateral distribution figure (7) for profile (WK) and figure (8) for profile (WKS). The lateral distribution revealed that, for profile (WK) there are three locations of high concentration of total heavy minerals in the 1st meter than that found in the 2nd meter. For profile (WKS) there is no distinct difference between two meters.

The distribution of the total economic minerals were graphically represented using lateral distribution figure (9) for profile (WK) and figure (10) for profile (WKS). The lateral distribution revealed that, there is no distinct difference between two meters in both profiles.

The high concentration of total heavy minerals in the 1st meter for profile (WK) caused as a result of the high surface concentration of green silicates because there is no a distinct difference between two meters in total economic minerals content.



Fig. 6: Shows the distribution of samples for profile (WK) and profile (WKS) on Google Earth photo.

Table 1: Percentages of total heavy bromoform for profile (WK) in the studied area.

Sample No	1st meter	2nd meter
	T.H.M. %	T.H.M. %
WK 1	8.43	5.73
WK 2	9.17	5.22
WK 3	6.12	4.73
WK 4	5.67	3.98
WK 5	5.44	3.88
WK 6	5.87	3.70
WK 7	7.96	4.87
WK 8	6.05	5.34
WK 9	5.12	4.26
WK 10	5.21	3.96
WK 11	4.44	4.38
WK 12	4.85	4.24
WK 13	6.28	5.16
WK 14	5.92	4.95
WK 15	7.37	3.98
WK 16	6.08	4.57
WK 17	6.30	4.22
WK 18	3.60	2.95
Min.	**3.60**	**2.95**
Max.	**9.17**	**5.73**
Aveg.	**6.10**	**4.45**

Table 2: Percentages of total heavy bromoform forprofile (WKS) in the studied area.

Sample NO	1st meter	2nd meter
	T.H.M. %	T.H.M. %
WKS 1	4.97	5.54
WKS 2	6.83	6.86
WKS 3	5.06	6.65
WKS 4	4.61	4.70
WKS 5	6.32	5.58
WKS 6	6.61	5.85
WKS 7	5.95	4.30
WKS 8	5.15	4.84
WKS 9	5.80	5.23
WKS 10	5.51	6.11
WKS 11	5.13	5.46
WKS 12	5.46	6.23
WKS 13	6.13	5.81
WKS 14	5.18	5.38
Min.	**4.61**	**4.30**
Max.	**6.83**	**6.86**
Aveg.	**5.62**	**5.61**

T.H.M.= Total heavy minerals

Table 3: Percentages of total economic minerals for the first meter in profile (WK) in the studied area.

Sample No	Mg.	Hem.	Ilm	Gar.	Leuc.	Rut.	Tit.	Zr.	Mz.	T.Ec. M. %	G.S. %	T.H. M. %
WK 1	0.584	0.020	1.150	0.103	0.075	0.041	0.008	0.076	0.008	2.07	6.37	8.43
WK 2	0.629	0.030	1.256	0.225	0.112	0.115	0.009	0.211	0.007	2.59	6.58	9.17
WK 3	0.527	0.002	0.972	0.169	0.079	0.099	0.006	0.136	0.006	2.00	4.12	6.12
WK 4	0.538	0.003	0.854	0.116	0.086	0.085	0.005	0.108	0.006	1.80	3.87	5.67
WK 5	0.352	0.002	0.931	0.109	0.025	0.047	0.003	0.101	0.004	1.57	3.87	5.44
WK 6	0.371	0.003	0.852	0.103	0.032	0.045	0.006	0.097	0.005	1.51	4.36	5.87
WK 7	0.411	0.002	0.998	0.093	0.078	0.071	0.008	0.080	0.006	1.75	6.21	7.96
WK 8	0.349	0.003	0.813	0.097	0.086	0.041	0.007	0.077	0.006	1.48	4.57	6.05
WK 9	0.378	0.002	0.788	0.087	0.071	0.055	0.007	0.079	0.005	1.47	3.65	5.12
WK 10	0.385	0.004	0.848	0.091	0.086	0.059	0.008	0.087	0.004	1.57	3.64	5.21
WK 11	0.370	0.003	0.833	0.084	0.053	0.027	0.007	0.064	0.006	1.45	2.99	4.44
WK 12	0.352	0.003	0.891	0.083	0.053	0.038	0.006	0.061	0.005	1.49	3.36	4.85
WK 13	0.392	0.002	0.887	0.081	0.060	0.031	0.006	0.073	0.003	1.54	4.75	6.28
WK 14	0.313	0.003	0.846	0.063	0.055	0.028	0.005	0.067	0.002	1.38	4.54	5.92
WK 15	0.463	0.002	0.966	0.072	0.046	0.023	0.006	0.056	0.004	1.64	5.73	7.37
WK 16	0.363	0.002	0.874	0.059	0.038	0.015	0.005	0.042	0.002	1.40	4.68	6.08
WK 17	0.371	0.002	0.819	0.063	0.049	0.056	0.005	0.060	0.002	1.43	4.87	6.30
WK 18	0.251	0.001	0.658	0.035	0.022	0.010	0.004	0.023	0.001	1.01	2.60	3.60
Min	0.251	0.001	0.658	0.035	0.022	0.010	0.003	0.023	0.001	1.01	2.60	3.60
Max	0.629	0.030	1.256	0.225	0.112	0.115	0.009	0.211	0.008	2.59	6.58	9.17
Ave.	0.411	0.005	0.902	0.096	0.061	0.049	0.006	0.083	0.005	1.62	4.49	6.10

Table 4: Percentages of total economic minerals for the second meter in profile (WK) in the studied area.

Sample No	Mg.	Hem.	Ilm	Gar.	Leuc.	Rut.	Tit.	Zr.	Mz.	T.Ec. M. %	G.S. %	T.H. M. %
WK 1	0.519	0.019	0.935	0.098	0.071	0.036	0.007	0.075	0.005	1.77	3.97	5.73
WK 2	0.512	0.002	0.863	0.154	0.082	0.037	0.005	0.084	0.003	1.74	3.48	5.22
WK 3	0.463	0.003	0.758	0.110	0.072	0.104	0.006	0.122	0.005	1.64	3.09	4.73
WK 4	0.516	0.002	0.858	0.107	0.081	0.063	0.004	0.095	0.005	1.73	2.25	3.98
WK 5	0.367	0.002	0.834	0.096	0.023	0.043	0.005	0.083	0.004	1.46	2.42	3.88
WK 6	0.346	0.003	0.833	0.099	0.029	0.038	0.007	0.096	0.005	1.46	2.24	3.70
WK 7	0.354	0.002	0.818	0.090	0.074	0.036	0.007	0.075	0.005	1.46	3.41	4.87
WK 8	0.337	0.003	0.784	0.094	0.081	0.038	0.005	0.073	0.004	1.42	3.92	5.34
WK 9	0.362	0.003	0.775	0.082	0.068	0.046	0.006	0.074	0.004	1.42	2.84	4.26
WK 10	0.379	0.003	0.812	0.086	0.080	0.043	0.007	0.074	0.004	1.49	2.47	3.96
WK 11	0.317	0.003	0.785	0.076	0.048	0.031	0.006	0.058	0.005	1.33	3.05	4.38
WK 12	0.326	0.002	0.864	0.075	0.045	0.023	0.005	0.052	0.004	1.40	2.84	4.24
WK 13	0.346	0.002	0.869	0.076	0.047	0.029	0.005	0.065	0.003	1.44	3.72	5.16
WK 14	0.276	0.002	0.694	0.048	0.034	0.010	0.006	0.025	0.002	1.10	3.85	4.95
WK 15	0.257	0.003	0.836	0.054	0.035	0.013	0.005	0.038	0.003	1.24	2.74	3.98
WK 16	0.233	0.002	0.736	0.034	0.021	0.018	0.006	0.037	0.002	1.09	3.48	4.57
WK 17	0.176	0.002	0.736	0.043	0.031	0.012	0.005	0.037	0.002	1.04	3.18	4.22
WK 18	0.112	0.001	0.437	0.290	0.014	0.009	0.003	0.016	0.001	0.88	2.07	2.95
Min	0.112	0.001	0.437	0.034	0.014	0.009	0.003	0.016	0.001	0.88	2.07	2.95
Max	0.519	0.019	0.935	0.290	0.082	0.104	0.007	0.122	0.005	1.77	3.97	5.73
Ave.	0.344	0.003	0.790	0.095	0.052	0.035	0.006	0.066	0.004	1.39	3.06	4.45

Table 5: Percentages of total economic minerals for the first meter in profile (WKS) in the studied area.

Sample No	Mg.	Hem.	Ilm	Gar.	Leuc.	Rut.	Tit.	Zr.	Mz.	T.Ec. M. %	G.S. %	T.H. M. %
WKS 1	0.387	0.001	0.652	0.119	0.109	0.051	0.004	0.096	0.006	1.43	3.55	4.97
WKS 2	0.398	0.001	0.763	0.117	0.105	0.056	0.005	0.095	0.005	1.55	5.29	6.83
WKS 3	0.343	0.002	0.711	0.103	0.096	0.036	0.005	0.094	0.004	1.39	3.67	5.06
WKS 4	0.317	0.001	0.620	0.098	0.094	0.034	0.004	0.085	0.003	1.26	3.35	4.61
WKS 5	0.341	0.002	0.660	0.097	0.088	0.034	0.005	0.097	0.003	1.33	4.99	6.32
WKS 6	0.366	0.003	0.784	0.097	0.091	0.035	0.005	0.096	0.004	1.48	5.13	6.61
WKS 7	0.313	0.002	0.721	0.081	0.079	0.029	0.004	0.063	0.003	1.30	4.66	5.95
WKS 8	0.296	0.001	0.693	0.081	0.075	0.025	0.004	0.058	0.003	1.24	3.91	5.15
WKS 9	0.323	0.002	0.700	0.077	0.073	0.025	0.003	0.058	0.003	1.26	4.54	5.80
WKS 10	0.297	0.001	0.633	0.067	0.063	0.019	0.004	0.051	0.003	1.14	4.37	5.51
WKS 11	0.261	0.002	0.607	0.074	0.061	0.011	0.004	0.043	0.002	1.07	4.07	5.13
WKS 12	0.288	0.001	0.657	0.078	0.067	0.016	0.003	0.041	0.002	1.15	4.31	5.46
WKS 13	0.302	0.002	0.715	0.076	0.072	0.018	0.006	0.041	0.005	1.24	4.89	6.13
WKS 14	0.287	0.001	0.658	0.077	0.061	0.017	0.003	0.043	0.002	1.15	4.03	5.18
Min	0.261	0.001	0.607	0.067	0.061	0.011	0.003	0.041	0.002	1.07	3.35	4.61
Max	0.398	0.003	0.784	0.119	0.109	0.056	0.006	0.097	0.006	1.55	5.29	6.83
Ave.	0.323	0.002	0.684	0.089	0.081	0.029	0.004	0.069	0.003	1.28	4.34	5.62

Table 6: Percentages of total economic minerals for the second meter in profile (WKS) in the studied area.

Sample No	Mg.	Hem.	Ilm	Gar.	Leuc.	Rut.	Tit.	Zr.	Mz.	T.Ec. M. %	G.S. %	T.H. M. %
WKS 1	0.412	0.001	0.761	0.122	0.115	0.067	0.005	0.103	0.006	1.59	3.95	5.54
WKS 2	0.423	0.002	0.768	0.110	0.108	0.049	0.005	0.083	0.004	1.55	5.31	6.86
WKS 3	0.376	0.001	0.752	0.110	0.100	0.046	0.005	0.097	0.004	1.49	5.16	6.65
WKS 4	0.327	0.001	0.618	0.093	0.091	0.030	0.004	0.075	0.003	1.24	3.46	4.70
WKS 5	0.334	0.001	0.651	0.094	0.083	0.033	0.004	0.092	0.003	1.30	4.29	5.58
WKS 6	0.341	0.002	0.765	0.092	0.084	0.032	0.004	0.090	0.003	1.41	4.44	5.85
WKS 7	0.287	0.002	0.654	0.077	0.063	0.023	0.003	0.056	0.003	1.17	3.13	4.30
WKS 8	0.288	0.001	0.672	0.076	0.071	0.022	0.003	0.053	0.003	1.19	3.65	4.84
WKS 9	0.308	0.001	0.656	0.073	0.067	0.021	0.004	0.055	0.002	1.19	4.04	5.23
WKS 10	0.275	0.001	0.587	0.061	0.056	0.015	0.003	0.046	0.003	1.05	5.06	6.11
WKS 11	0.254	0.001	0.587	0.071	0.055	0.009	0.003	0.038	0.002	1.02	4.44	5.46
WKS 12	0.272	0.001	0.638	0.072	0.061	0.013	0.004	0.036	0.002	1.10	5.13	6.23
WKS 13	0.187	0.001	0.525	0.065	0.053	0.010	0.004	0.032	0.002	0.88	4.93	5.81
WKS 14	0.173	0.001	0.540	0.056	0.042	0.008	0.003	0.038	0.001	0.86	4.52	5.38
Min	0.173	0.001	0.525	0.056	0.042	0.008	0.003	0.032	0.001	0.86	3.13	4.30
Max	0.423	0.002	0.768	0.122	0.115	0.067	0.005	0.103	0.006	1.59	5.31	6.86
Ave.	0.304	0.001	0.655	0.084	0.075	0.027	0.004	0.064	0.003	1.22	4.39	5.61

S. No.=Sample number, **Mgt.**=Magnetite, **Hem.**= hematite, **Ilm.**=Ilmenite, **Gar.**=Garnet, **Leuc.**=leucoxene, **Rut.**=Rutile, **Tit.**= titanite (Sphene), **Zr.**=Zircon, **Mz.**=Monazite, **T.Ec.M.**= Total Economic Mineral **G.S.**=Green silicates and **T.H.M.**= Total heavy minerals**.**

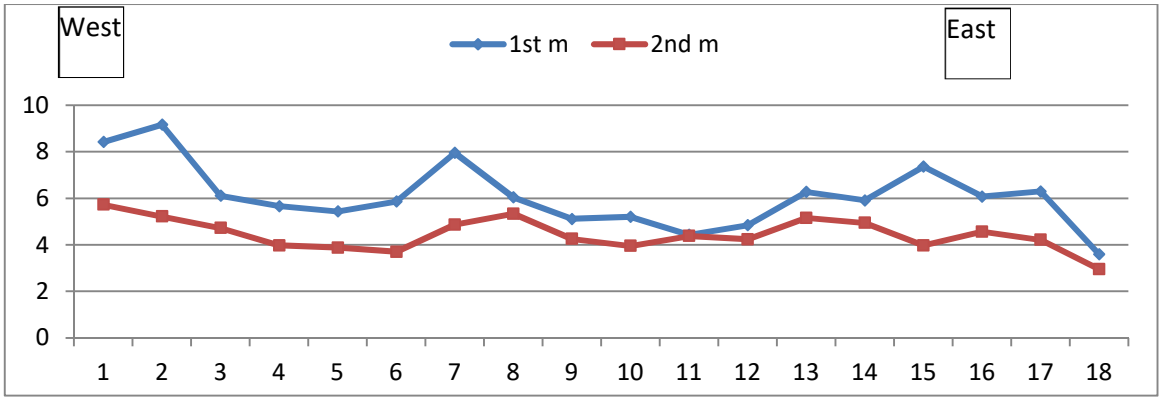


Fig. 7: Lateral distribution of total heavy minerals for profile (WK) in the study area.

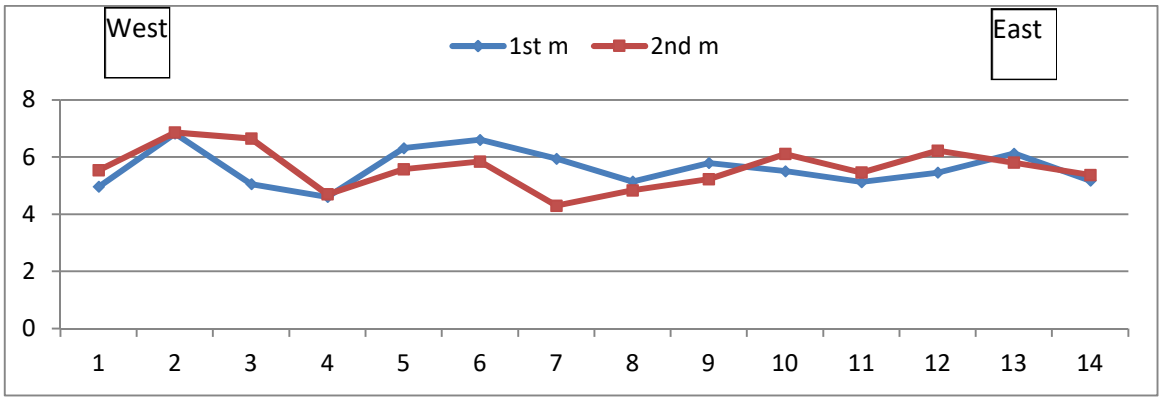


Fig. 8: Lateral distribution of total heavy minerals for profile (WKS) in the study area.

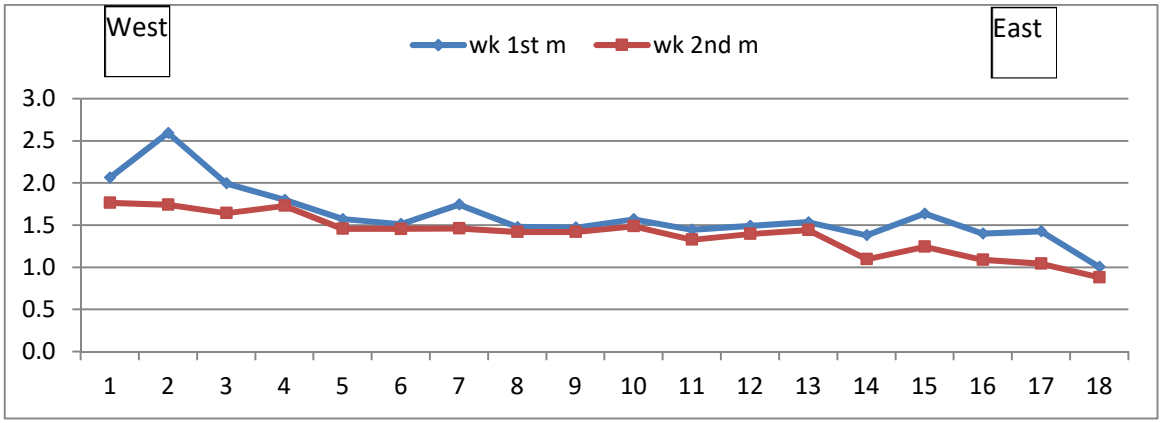


Fig. 9: Lateral distribution of total economic minerals for profile (WK) in the study area

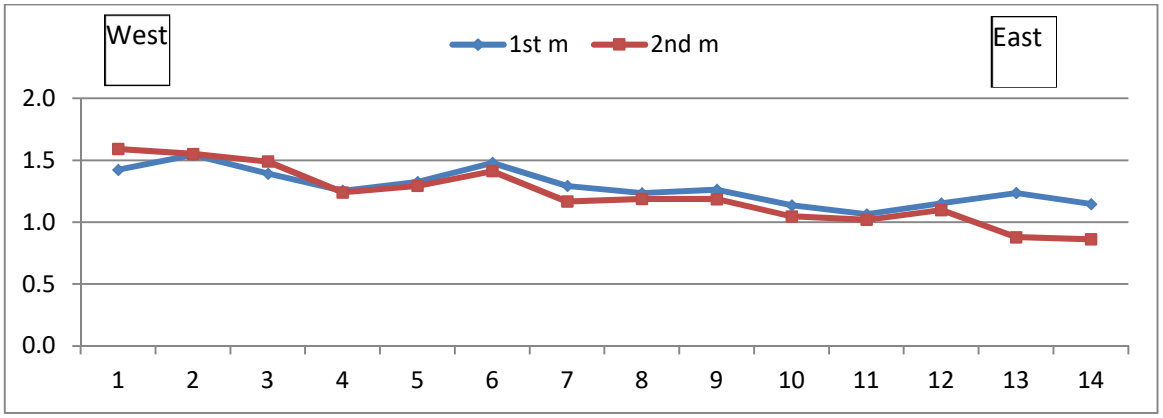


Fig. 10: Lateral distribution of total economic minerals for profile (WKS) in the study area.

Microscopic Study
The opaque minerals
Magnetite (Fe_3O_4)

Magnetite displays black to deep reddish-brown color, with metallic to dull luster. The brownish tint can be attributed to their alteration and/or oxidation process which were studied previously by many workers (El Balakssy 2003, Mansour 2009 and Barakat 2016).

Due to heterogeneous sources of the Egyptian black sand magnetite, it contains considerable amount of titano-magnetite in addition to small amounts of manganese, vanadium, and chromium rich varieties. The titanium free Magnetite forms only about 15 wt. % of the total Egyptian magnetite (Wassef and Mikhail, 1981).

Magnetite content in the 1st meter in profile (WK) range from 0.251% to 0.629% with an average of 0.411% (Table 3), in the 2nd meter in the same profile range from 0.112% to 0.519% with an average of 0.344% (Table 4). Its content in the 1st meter in profile (WKS) range from 0.261% to 0.398% with an average of 0.323% (Table 5), in the 2nd meter in the same profile range from 0.173% to 0.423% with an average of 0.304% (Table 6).

Magnetite habit ranges from massive, granular, angular to sub-angular (Fig. 11a). Picked pure magnetite grains were investigated under the Environmental Scanning Electronic Microscope (ESEM) and the elemental chemical compositions are shown in figure (11b), Titano-magnetite contains up to 13% TiO2 (Ward and Towner 1985) in the present study the EDX of magnetite (semi quantitative chemical analysis) shows additional weight percent of titanium reaches up to 16.83%. The titano-magnetite minerals such as magnetite, ilmenite, leucoxene and rutile are mainly derived from the mafic volcanic rocks of the Blue Nile provenance beside gold traces (El-Kammar *et al*., 2010). Pure magnetite grains were shown in figure (11b)

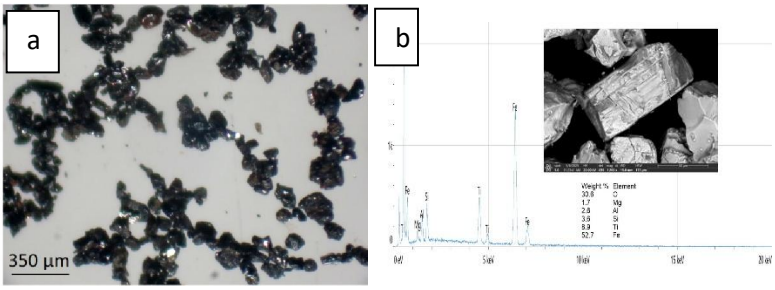


Fig. 11: Photomicrographs of magnetite grains show: a) Aggregates of sub-angular and sub-rounded grains, b) EDX and BSE image of magnetite grains

Hematite (Fe_2O_3)

Hematite is the principle ore of iron which originated mainly from magnetite alteration processes and alteration product of many Fe-bearing minerals especially pyrite and so-called hematite after pyrite (goethite) or pseudomorphic pyrite. The non-crystalline forms of hematite are supposedly transformations of the mineral limonite and occurs as a reddish brown to black color (Fig. 12a &b).

Hematite content in the 1st meter in profile (WK) range from 0.001% to 0.030% with an average of 0.005% (Table 3), in the 2nd meter in the same profile range from 0.001% to 0.019% with an average of 0.003% (Table 4). Its content in the 1st meter in profile (WKS) range from 0.001% to 0.003% with an average of 0.002% (Table 5), in the 2nd meter in the same profile range from 0.001% to 0.002% with an average of 0.001% (Table 6).

Pure hematite grains were investigated under the Environmental Scanning Electronic Microscope (ESEM) and the elemental chemical compositions are shown in figure (12c). It was recorded in all studied sediments as common accessory mineral.



Fig. 12: Photomicrographs show: a &b) granular, angular to sub-angular hematite and c) EDX and BSE image of hematite grains

Ilmenite ($FeO.TiO_2$)

Ilmenite was recorded as iron-black with metallic luster. Figure (13 a) shows different aggregates and different shapes of ilmenite, it occurs as elongated grains (Fig. 13 b), irregular angular to subangular with sharp edges (Fig. 13c), oval shape and well rounded to subrounded grains (Fig. 13d), discoidal grains with pitted surface (Fig. 13e) and chevron shape (Fig. 13f).

Ilmenite is considered as the most important ore of titanium, consequently, it is used as a raw material for pigment production, paints, printing inks, plastics, rubber, artificial fibers, paper, glass and ceramics (Elsner, 2010). Ilmenite is a ferromagnetic mineral separated mainly at the magnetic fields 0.2A and 0.5A. The significance of ilmenite as the most important rock-forming titanium mineral is not due to titanium extraction but for the production of titanium dioxide (TiO_2), so it is economically important and considered as a major source of titanium and a minor source of iron (Zhang *et al*., 2011).

Ilmenite content in the 1st meter in profile (WK) range from 0.658% to 1.256% with an average of 0.902% (Table 3), in the 2nd meter in the same profile range from 0.437% to 0.935% with an average of 0.790% (Table 4). Its content in the 1st meter in profile (WKS) range from 0.607% to 0.784% with an average of 0.684% (Table 5), in the 2nd meter in the same profile range from 0.525% to .0768% with an average of 0.655% (Table 6).

Pure ilmenite grains were investigated under the Environmental Scanning Electronic Microscope (ESEM) and the elemental chemical compositions are shown in figure (13g & h).

Leucoxene

The alteration process of ilmenite is accompanied by change in their chemical and physical properties. Chemically the main results of alteration process are an increase in TiO_2, Fe_2O_3 and H_2O and a decrease in FeO. Leucoxination process does not only affect the overall grade, but also changes the density of mineral grains and their magnetic susceptibility. Both SiO_2 and Al_2O_3 impurity levels in the grains increase with increasing of leucoxination degree (Hugo and Cornell, 1991).

The leucoxene commonly occurs as rounded grains, opaque in transmitted light. A rough pitted surface is characteristic of most grains. The color of leucoxene grains from the Egyptian black sands varies from light to dark brown color with different forms (Fig. 14a &b), plat (Fig. 14c) and represented dark brown with remaining of black ilmenite (Fig. 14d). The color depends mainly on the degree of alteration.

Leucoxene content in the 1st meter in profile (WK) range from 0.022% to 0.112% with an average of 0.061% (Table 3), in the 2nd meter in the same profile range from 0.014% to 0.082% with an average of 0.052% (Table 4). Its content in the 1st meter in profile (WKS) range from 0.061% to 0.109% with an average of 0.081% (Table 5), in the 2nd meter in the same profile range from 0.042% to 0.115% with an average of 0.075% (Table 6).

Picked leucoxene grains were investigated using ESEM and their chemical composition is shown in figure (14) which shows rounded grains (Fig. 14e), and relicts of ilmenite in leucoxene grains (Fig. 14f).

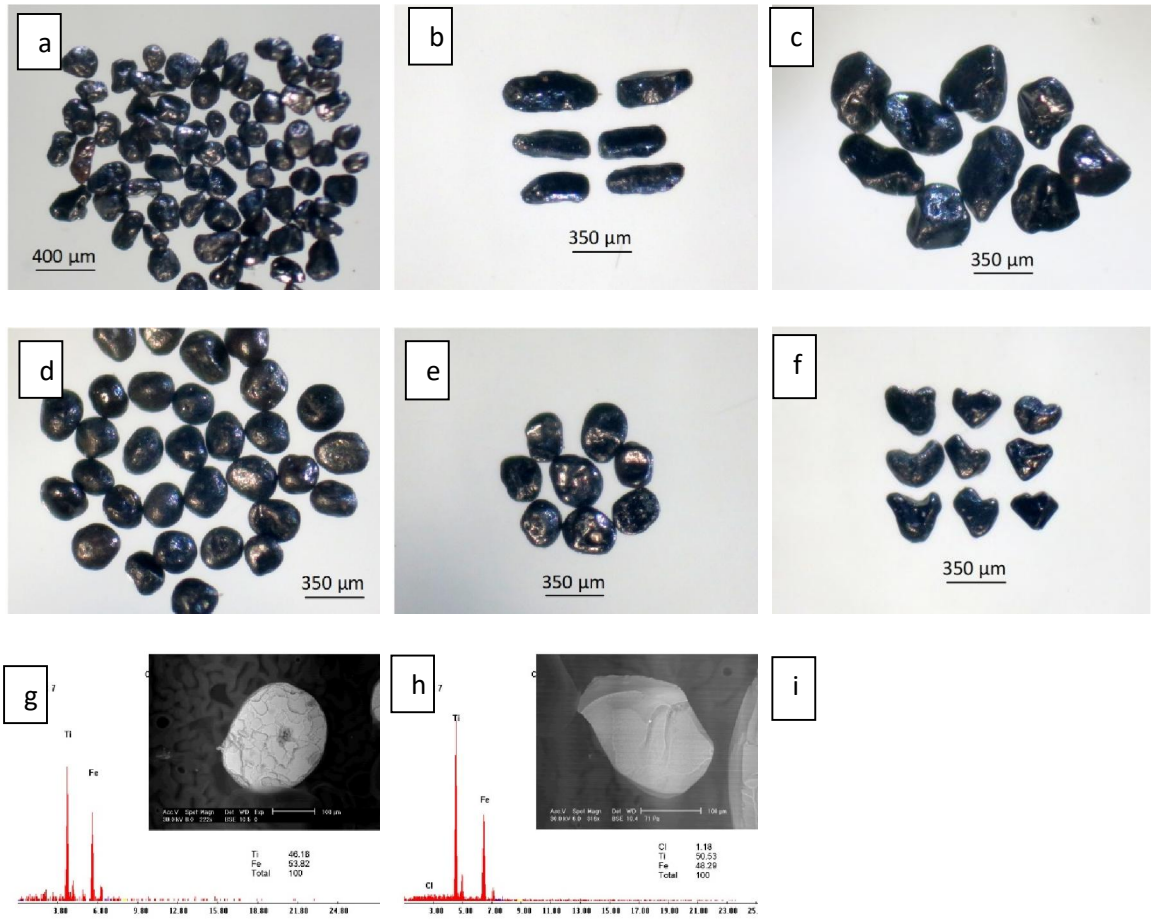


Fig. 13: photomicrograph shows: a) different aggregates and different shapes of ilmenite, b) elongated grains, c) irregular angular to subangular with sharp edges, d) oval shape and well rounded to subrounded, e) discoidal grains with pitted surface, f) chevron shape, and g & h) EDX and BSE image of ilmenite grains.

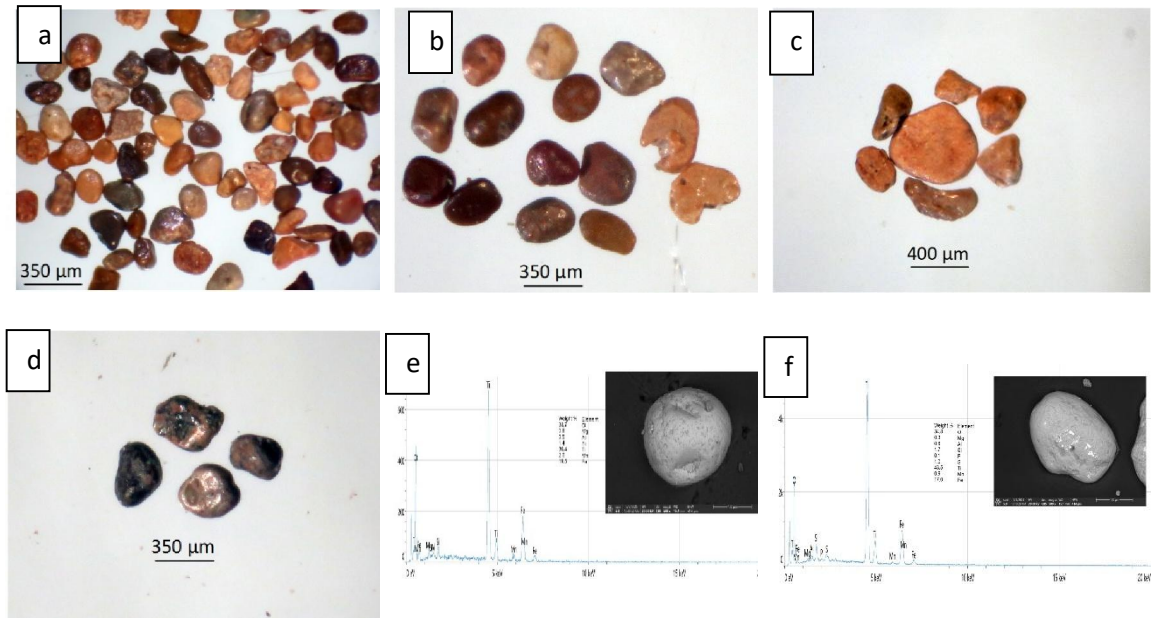


Fig. 14: Photomicrographs shows: a &b) light to dark brown color with different forms, c), plat, d) dark brown with remaining of black ilmenite and e &f) EDX and BSE image of leucoxene grains.

The Non-opaque minerals

Garnet

Garnet is a group of minerals closely have physical and chemical properties. The minerals of garnet group characterize some metamorphic rocks, others occur in high-pressure igneous rocks. The more common color for Egyptian black sand garnet is the pale pink. Garnet has moderate magnetic susceptibility which varies slightly according to variation in chemical composition (Milner, 1962).

Garnet was recorded in the all studied samples as different colors and shapes (Fig. 15a), colorless (Fig. 15b), angular rose (Fig. 15c), rose garnet with different degree of inclusions which change its color from colorless to black (Fig. 15d), red (Fig. 15e), sub-rounded to well-rounded and euhedral grains (Fig 15f) and green tsavorite garnet (Fig. 15 g).

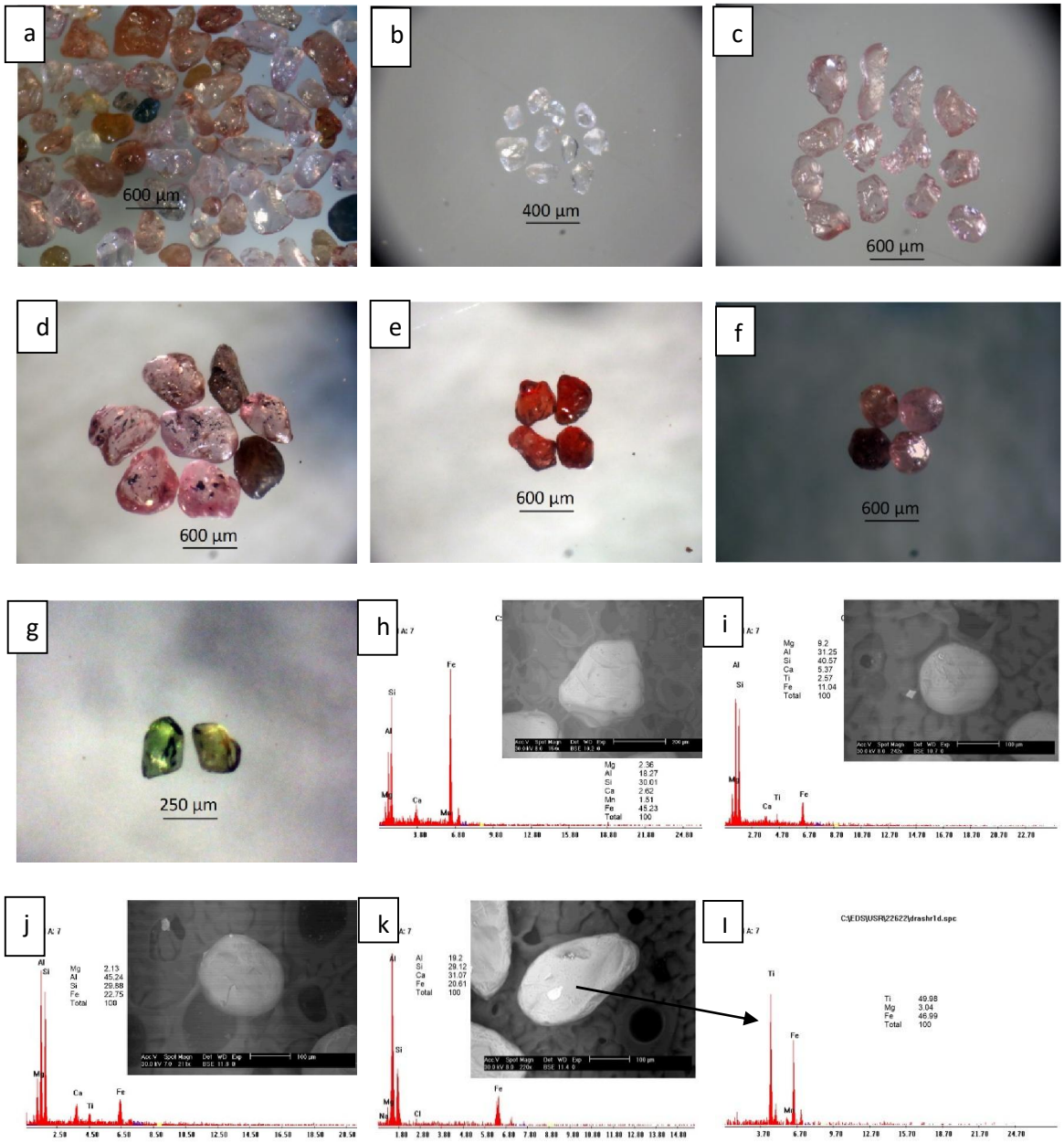


Fig. 15: Photomicrographs show: a) different colors and shapes, b) colorless, c) angular rose, d) rose garnet with different degree of black inclusions which change its color from colorless to black, e) red, f) sub-rounded to well-rounded and euhedral grains, g) green tsavorite garnet, h & I &j) EDX and BSE image of almandine garnet, k) EDX and BSE image of almandine-grossular solid solution garnet with ilmenite inclusions (l).

Garnet content in the 1st meter in profile (WK) range from 0.035% to 0.225% with an average of 0.096% (Table 3), in the 2nd meter in the same profile range from 0.034% to 0.290% with an average of 0.095% (Table 4). Its content in the 1st meter in profile (WKS) range from 0.067% to 0.119% with an average of 0.089% (Table 5), in the 2nd meter in the same profile range from 0.056% to 0.122% with an average of 0.084% (Table 6).

Pure garnet grains were investigated under the Environmental Scanning Electronic Microscope (ESEM) and the elemental chemical compositions are shown in Figures (15). The analyzed garnet grains are represented mainly by almandine ($Fe_3Al_2Si_3O_{12}$) as a major component (Fig. 15h, I and j) and almandine-grossular solid solution (Fig. 15k) with ilmenite inclusion (Fig. 15l).

Zircon

Egyptian black sand zircon exhibits a peculiar behavior in regards to its magnetic susceptibility. This is due to the presence of inclusions which are different in quantity and in nature. Rittman and Nakhla (1958) classified the black sand zircon into, strongly magnetic (1 wt.%), moderately magnetic (8 wt. %) and non-magnetic (91wt.%).

According to Rozendaal & Philander (2000), zircon can be grouped into four types as follow:- a) Clear zircons contain low levels of Fe, U and Th. b) Pink zircons contain moderate levels of rare earths (REE), U and Th.) Yellow zircons contain high levels of REE, U, Th, Fe, Al, P and Ca and d) Metamict zircons contain very high levels of REE, U, Th, Fe and Y.

Most of zircon grains have euhedral external morphology. It was recorded as colorless short to long prismatic with or without bi-pyramid termination (Fig. 16a), colorless sub-rounded to rounded (Fig. 16b), white oval grains (Fig. 16c), white prismatic with smooth curved edges (Fig. 16d), reddish yellow and red prismatic (Fig. 16e &f) and honey color (Fig. 16g).

The variation in the color of zircon may be attributed to the density of fine inclusions as well as the degree of iron oxides staining. Some inclusions may be due to iron ions that could penetrate from the original melt through zircon lattice during magmatic crystallization or from an outside source. These inclusions are considered as weak points which accelerate the disintegration of the grains (Hassan 2005 and Surour *et al*., 2003).

Zircon content in the 1st meter in profile (WK) range from 0.023% to 0.211% with an average of 0.083% (Table 3), in the 2nd meter in the same profile range from 0.016% to 0.122% with an average of 0.066% (Table 4). Its content in the 1st meter in profile (WKS) range from 0.041% to 0.097% with an average of 0.069% (Table 5), in the 2nd meter in the same profile range from 0.032% to 0.103% with an average of 0.064% (Table 6).

Pure zircon grains were investigated under the Environmental Scanning Electronic Microscope (ESEM) and the elemental chemical compositions are shown in Figures (16h, I, j &k).

Rutile

Rutile is one of the three polymorphs of titanium dioxide, rutile, anatase and brookite. It considered the most common forms of TiO_2 in nature. Hammoud (1966) classified the rutile in the Egyptian black sand to different classes, 2.9 wt.% opaque ilmenorutile, 4.2 wt.% ferriferous rutile, 6.1 wt.% ex-translucent ilmenorutile, 19.8 wt. % secondary rutile and 67 wt.% translucent rutile.

Rutile has a wide range of magnetic susceptibilities. It concentrates in the low magnetic fields according to its iron content. Egyptian beach rutile is transparent, translucent and opaque. The Egyptian rutile particles appear under the binocular stereomicroscope as aggregates of different color and shapes (Fig. 17a), small prismatic euhedral to subhedral grains with red to black color (Fig. 17b), rounded and oval (Fig. 17c) and chevron shape (Fig. 17d).

Rutile content in the 1st meter in profile (WK) range from 0.010% to 0.115% with an average of 0.049% (Table 3), in the 2nd meter in the same profile range from 0.009% to 0.104% with an average of 0.035% (Table 4). Its content in the 1st meter in profile (WKS) range from 0.011% to 0.056% with an average of 0.029% (Table 5), in the 2nd meter in the same profile range from 0.008% to 0.067% with an average of 0.027% (Table 6).

Pure rutile grains were investigated under the Environmental Scanning Electronic Microscope (ESEM) and the elemental chemical compositions are shows that; pure rutile grain (Fig. 17e &f).

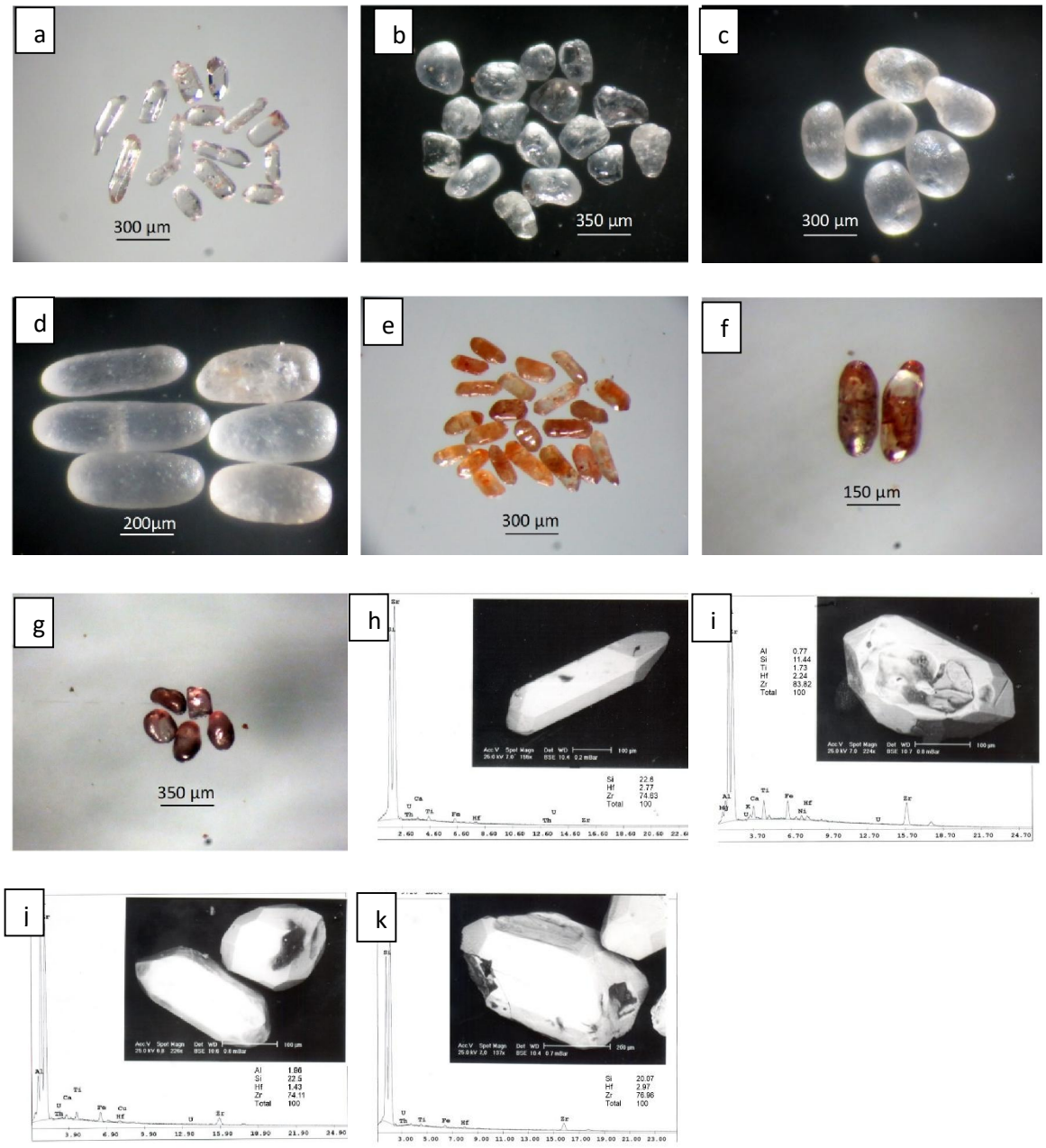


Fig. 16: Photomicrographs show: a) colorless short to long prismatic with or without bi-pyramid termination, b) colorless sub-rounded to rounded, c) white oval grains, d) white prismatic with smooth curved edges, e) reddish yellow and red prismatic, f) honey color, h& i& j& k) EDX and BSE image of zircon.

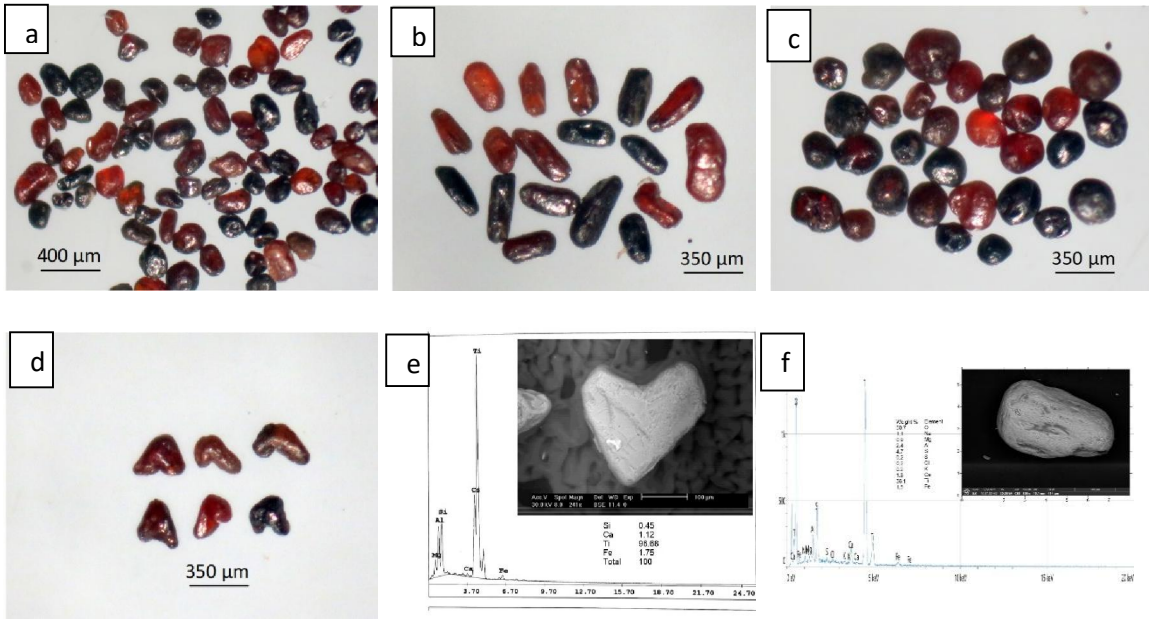


Fig. 17: Photomicrographs show: a) aggregates of different color and shapes, b) small prismatic euhedral to subhedral grains with red to black color, c) rounded and oval, d) chevron shape, e &f) EDX and BSE image of rutile.

Monazite

Monazite is one of the most important nuclear minerals, being a major host for REEs and actinides Th and U. The Egyptian beach monazite occurs as very well-rounded grains, mostly taking the oval shape with high sphericity. It is free from inclusions and has colors varying from colorless to deep brown. Zaghloul and Kamel (1965) identified six color varieties of the Egyptian beach monazite, they are brown, yellowish brown, reddish brown, yellow, honey yellow and lemon yellow. They concluded that, the two principal colors of this mineral are the lemon yellow (59%) and the honey-yellow ones (25%). Monazite is essentially a phosphate of rare earth mainly cerium, thorium and uranium in which thorium and yttrium substitute for cerium. Moustafa and Abdel Fattah, (2010) reported that the Egyptian beach monazite is colorless to pinkish in color and mostly derived from highly differentiated granite. Moreover, believed that the monazite of the Egyptian black sand is almost exclusively supplied by the White Nile.

Their color ranges from colorless, lemon yellow, light red and deep red and its shape occur as rounded and discoidal (Fig. 18a) and elongated and oval grains (Fig. 18b). They occur as accessory mineral in the fine and very fine sand fractions. It was separated at magnetic field strength 0.5A and 1.0A. Monazite exhibits shape varies between rounded, discoidal, oval and prismatic.

In reality, monazite technically four different minerals technically, but because of a lack of great differences between them they are referred to as one mineral monazite. The four monazites have differences in the percentages of their chemical constituents. Their differences are reflected in their respective names (Van Emden *et al*., 1997):

(Ce)-Monazite: (Ce, La, Nd, Th, Y)PO_4
(La)-Monazite: (La, Ce, Nd)PO4
(Nd)-Monazite: (Nd, La, Ce)PO4
(Sm)-Monazite: (Sm, Gd, Ce, Th)PO_4

Monazite content in the 1st meter in profile (WK) range from 0.001% to 0.008% with an average of 0.005% (Table 3), in the 2nd meter in the same profile range from 0.001% to 0.005% with an average of 0.004% (Table 4). Its content in the 1st meter in profile (WKS) range from 0.002% to 0.006% with an average of 0.003% (Table 5), in the 2nd meter in the same profile range from 0.001% to 0.006% with an average of 0.003% (Table 6).

Pure monazite grains were investigated under the Environmental Scanning Electronic Microscope (ESEM) and the elemental chemical compositions are shown in figures (18c). All monazite of the studied sediments belongs to (Ce)-Monazite.

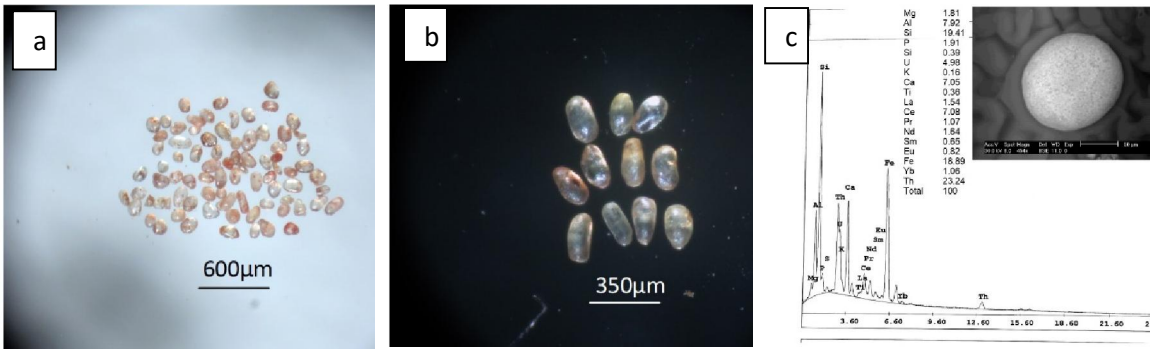


Fig. 18: Photomicrographs show: a) rounded and discoidal monazite, b) elongated and oval monazite and c) EDX and BSE image of monazite.

Titanite (Sphene) (CaTiSiO5)

Titanite is more common in all samples of the studied sediments. Its color varies from yellowish to brownish yellow with vitreous luster (Fig. 19) and its shape occur as angular to sub-angular (Fig. 19a &b), rounded and oval grains (Fig. 19c) and euhedral grains (Fig. 19e). Titanite mineral grains are subhedral to anhedral grains with imperfect cleavage. Titanite was separated at magnetic field strength 1.0A and less common in 0.5A.

Titanite content in the 1st meter in profile (WK) range from 0.003% to 0.009% with an average of 0.006% (Table 3), in the 2nd meter in the same profile range from 0.003% to 0.007% with an average of 0.006% (Table 4). Its content in the 1st meter in profile (WKS) range from 0.003% to 0.006% with an average of 0.004% (Table 5), in the 2nd meter in the same profile range from 0.003% to 0.005% with an average of 0.004% (Table 6).

Pure titanite grains were investigated under the Environmental Scanning Electronic Microscope (ESEM) and the elemental chemical compositions are shown in Figure (19e)

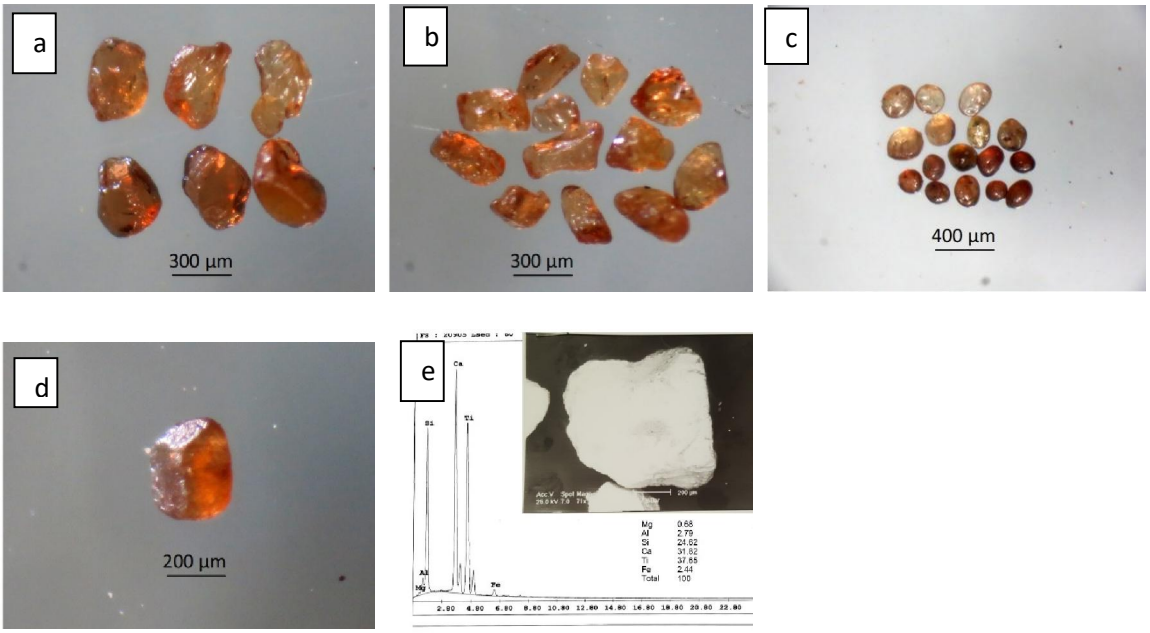


Fig. 19: Photomicrographs show: a &b) angular to sub-angular, c) rounded and oval grains, d) euhedral grains and e) EDX and BSE image of titanite.

Accessory minerals

Staurolite (Fe_2^{+2} Al_9 O_6 $(SiO_4)_4(O, OH)_2$)

Staurolite grains $(Fe,Mg)_2$ $(Al,Fe)_9$ O_6 $(SiO_4)(OOH)$ were separated at magnetic field strength 0.2A and 0.5A and were picked using binocular stereomicroscope. Barakat (2016) stated that: Staurolite represent about 3% of garnet concentrate and it has been used as an abrasive. Staurolite occur as yellow grains (Fig. 20a). Pure staurolite grains were investigated under the Environmental Scanning Electronic Microscope (ESEM) and the elemental chemical compositions are shown in figure (20b).

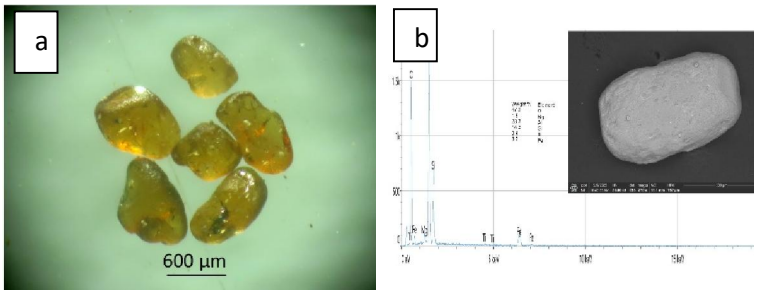


Fig. 20: Photomicrographs shows: a) Yellow staurolite grains and b) EDX and BSE image of staurolite.

Pyrite (FeS2)

Pyrite is one of the few minerals that are produced by biological micro-environmental systems. It is a common sulphide mineral together with chalcopyrite. Framboidal pyrite is frequent in the investigated sediments. It has well developed rounded shape with two variant colors, as were as golden yellow or shiny brassy yellow (Fig. 21a &b). Pure pyrite grains were investigated under the Environmental Scanning Electronic Microscope (ESEM) are shown in (Fig. 21c) which its EDX shows the pure composition. Pyrite was separated at magnetic field strength 1.5A using the Frantz Isodynamic separator.

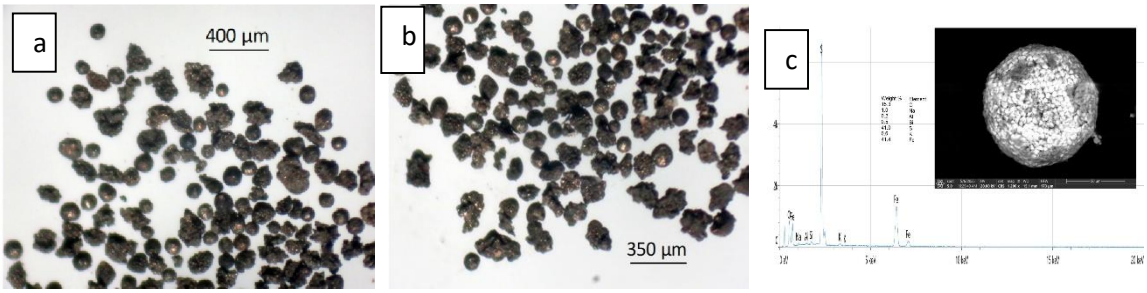


Fig. 21: Photomicrographs show: a &b) Golden yellow pyrite and c) EDX and BSE image of pyrite.

Apatite Ca_5 $(PO_4)_3F$

Apatite is the most common phosphate mineral, representing the main source of phosphorus required to plants. Furthermore, it represents the main component of the bones and teeth of most animals, including humans. It was recorded in the studied samples as road like, wedge, platy and irregular shape with brown color (Fig. 22a &b). Pure apatite grains were investigated under the Environmental Scanning Electronic Microscope (ESEM) and the elemental chemical compositions are shown in Figure (22c) with zircon inclusion (Fig. 22d).

Chromite $FeCr_2O_4$

Chromite is the main ore of chromium and has a wide range in industrial uses. It is used as a refractory material due to its high heat stability. Chromite usually occurs as well-formed octahedron crystals. It was separated at 0.2A and 0.5A using Frantz Isodynamic Separator. Its color varies from black to brownish black with metallic luster (Fig. 23a). Pure chromite grains were investigated under the Environmental Scanning Electronic Microscope (ESEM) and the elemental chemical compositions are shown in figure (23b).

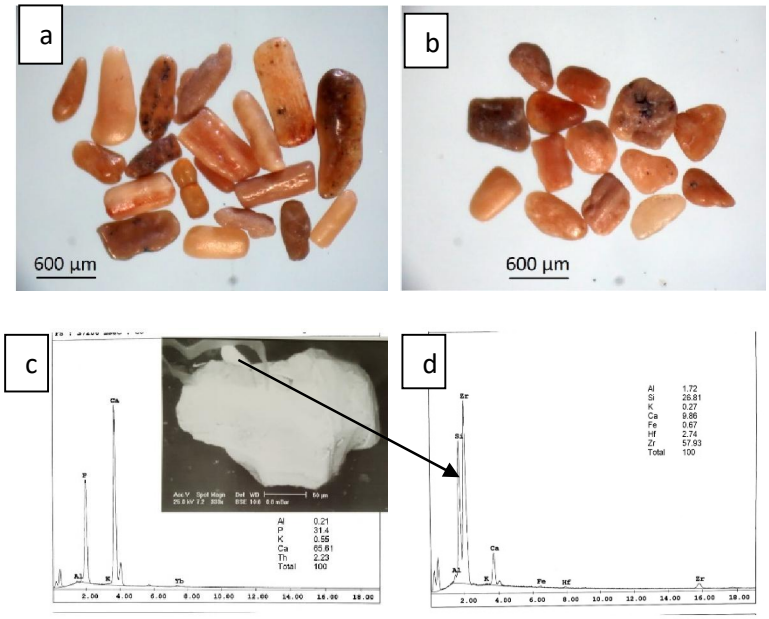


Fig. 22: Photomicrographs shows: a &b) apatite and c) EDX and BSE image of apatite with zircon inclusion (d).

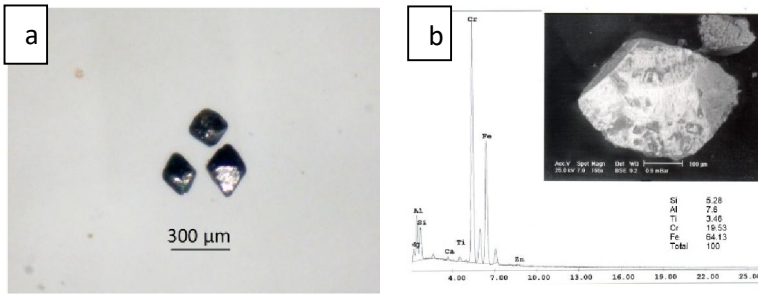


Fig. 23: Photomicrographs shows: a) Octahedron chromite and b) EDX and BSE image of chromite.

Kyanite Al_2SiO_5

This mineral is one of the kyanite, sillimanite, andalusite metamorphic mineral group. Kyanite show blue, white and rarely green color, transparent to translucent (Fig. 24a &b), The crystal habit ranges from columnar; fibrous; bladed, vitreous to pearly luster, and perfect cleavage. Pure kyanite grains were investigated under the Environmental Scanning Electronic Microscope (ESEM) and the elemental chemical compositions are shown in figure (24c). Kyanite is commonly found in aluminum-rich metamorphic pegmatites and/or sedimentary rock. Kyanite in metamorphic rocks generally indicates pressures higher than 4 kb

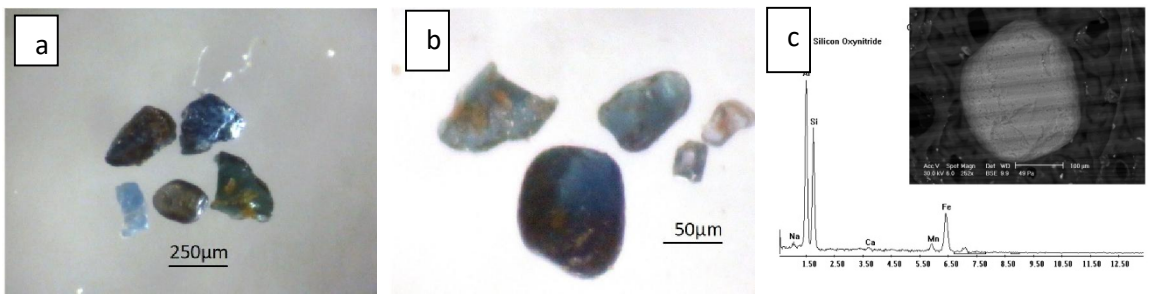


Fig. 24: Photomicrographs shows: a &b) gahnite and c) EDX and BSE image of gahnite.

Green Silicates

The green silicates are common minerals in these sediments, and separated using heavy liquid bromoform (sp. gr. 2.86 gm/cm3). It is mainly concentrated in the first magnetic fraction 0.2A and the rest found in 0.5A and decreases with increasing of magnetic field strength.

This mainly fraction includes silicate with sheet structure as mica including muscovite and biotite, silicate with single chain pyroxene group comprising five important minerals (bronzite, hyperthene, diopside, hedenbergite, augite, aegirine, and jadeite) which are altered to carbonates or chlorite minerals, and double chain amphiboles group which contain anorthphyllite, tremolite, actinolite, cummingtonite, hornblende, glaucophane, riebeckite, and arfvedsonite, which are altered to serpentine or chlorite or carbonate. This is in addition to silicate with isolated tetrahedral as olivine group, and less common kyanite, sillimanite, andalusite, and staurolite, and isolated double tetrahedral epidote group.

4. Conclusion

The study area extend from East El Gharbia drainage from the West to new El Mansoura city from the East with total length of about 18km, while the width extend from the beach southward to the International High way ranging from 0.750km to 1.60km with total area of about 24.50km^2. This study is mainly concerned to the muddy coast. The coastal environment is the area lying at the interface between the land and the sea.

The area is covered by two profiles oriented parallel to the shoreline with 1 km spacing. About 32 stations were drilled in east El-Gharbia drainage using auger equipment for two-meter depth in every station. The first profile located near the shore and include 18 stations by total samples of 36 referred by simple (WK). the second profile located southward the first one and near to the International High way and include 14 stations by total samples of 28 referred by simple (WKS), so the total samples which collected from the area are 64 samples.

The distribution of the total heavy minerals between 1st and 2nd meter were graphically represented using lateral distribution which revealed that, for profile (WK) there are three locations of high concentration of total heavy minerals in the 1st meter than that found in the 2nd meter. For profile (WKS) there is no distinct difference between two meters.

The distribution of the total economic minerals were graphically represented using lateral distribution which revealed that, there is no distinct difference between two meters in both profiles. The high concentration of total heavy minerals in the 1st meter for profile (WK) caused as a result of the high surface concentration of green silicates because there is no a distinct difference between two meters in total economic minerals content.

The identified heavy mineral assemblages studied under a Binocular Stereomicroscope in the studied area can be classified into two main groups according to Folk (1980). The first one includes opaque minerals as; Magnetite, Hematite, Ilmenite, Leucoxene. The second group comprises non-opaque minerals includes Garnet, Zircon, Rutile, Monazite and Titanite. The accessory minerals as: Staurolite, Pyrite, Apatite, Chromite, kyanite and Green Silicate minerals.

References

Awad, M., A. M. El Mezayen, S. M. El Alfi, H. H. Ali, M. I. Sayyed and M. Y. Hanfi, 2023. Separation, reserve estimation and radioactivity responsibility of the economic heavy minerals of East El-Arish black sand, North Sinai, Egypt. Sci. Rep., 13:4608.

Barakat, M. G., 2016. Evaluation and mineralogy of beach economic minerals especially ilmenite for the top meter in the Egyptian black sand, east Rosetta, Egypt. Ph.D. Thesis, Fac. Sci., Zagazig Univ., Egypt, 284 p.

El-Afandy A. H., M. I. Moustafa, H. A. El-Nahas, A. A. Abdou and M. G. Barakat, 2016. Geomorphology and mineralogy of the top meter black sands north west of El-Burullus Lake, Kafr Al-Sheikh Governorate, Egypt. Al-Azhar Bull. Sci., 27(2):65-72.

El Afandy, A., M. Khalil, A. El Azab, S. El Alfi, M. Etman and H. R. Saad, 2022. Throw light on the heavy economic minerals of the northern part of Delta, Egypt. Middle East J. Appl. Sci., 12(4):553-581.

El Alfi, S. M., 2019. Inferred resources of heavy economic minerals in West El Burullus area, Egypt. J. Sedimentol. Soc. Egypt, 24:129-147.

El Alfi, S. M., M. M. Abdel-Azeem, H. H. Ali and M. H. Soliman, 2023. Prospectivity of economic heavy minerals from El Manzala bottom sediments, North Nile Delta, Egypt. Curr. Sci. Int., 12(2):151-167.

El Azab, A., S. M. El Alfi and H. H. Ali, 2018. Mineralogy and radioactivity of the southern part of Nasser Lake sediments, Egypt. Al-Azhar Bull. Sci., 29(2):143-163.

El Azab, A., S. M. El Alfi and H. H. Ali, 2019. Economic heavy minerals evaluation of Damietta harbor channel sediments, Egypt. J. Sedimentol. Soc. Egypt, 24:43-61.

El Balakssy, S. S., 2003. Mineralogical studies for the economic minerals in the sand dunes belt at Baltim area, Egypt. Ph.D. Thesis, Fac. Sci., Ain Shams Univ., Egypt.

El Rakaiby, M. L. and N. Attia, 2004. Morphological and geological classification of the Egyptian northern coastal environment using space image technology. Bull. Soc. Geogr. Egypte, 77:1-18.

El-Hadary, A. F., 1998. Geological, sedimentological and radiometric studies on the black sand deposits, west Rosetta beach with emphasis on the heavy economic minerals. Ph.D. Thesis, Fac. Sci., Cairo Univ., Egypt.

El-Kammar, A. A., A. A. Ragab and M. I. Moustafa, 2010. Geochemistry of economic heavy minerals from Rosetta black sand of Egypt. J. King Abdulaziz Univ. Earth Sci., 21(2):1-25.

Elsner, H., 2010. Heavy minerals of economic importance. Assessment Manual, Federal Institute for Geosciences and Natural Resources (BGR), Hannover, Germany, 218 p.

Folk, R. L., 1980. Petrology of Sedimentary Rocks. Hemphill Publishing Company, Austin, Texas, USA, 184 p.

Hammoud, N. S., 1966. Concentration of monazite from Egyptian black sand, employing industrial techniques. M.Sc. Thesis, Fac. Sci., Cairo Univ., Egypt.

Hugo, V. E. and D. H. Cornell, 1991. Altered ilmenites in Holocene dunes from Zululand, South Africa: Petrographic evidence for multistage alteration. S. Afr. J. Geol., 94(5-6):365-378.

Keller, E. A., 2000. Environmental Geology. 8th Ed., Prentice Hall, Upper Saddle River, New Jersey, USA, 562 p.

Mansour, S. M. M., 2009. Geology, mineralogy and radioactivity studies on Nuweibi area, Central Eastern Desert, Egypt. M.Sc. Thesis, Fac. Sci., Benha Univ., Egypt.

Milner, H. B., 1962. Sedimentary Petrography. Vol. II, George Allen & Unwin Ltd., London, UK, 715 p.

Moustafa, M. I. and N. A. Abdel Fattah, 2010. Physical and chemical beneficiation of the Egyptian beach monazite. Resour. Geol., 60(3):288-299.

Ragab, H., A. H. El Afandy, M. Khalil and A. Yousry, 2017. Inferred resources and environmental impact of the top meter black sands in the coastal area of Mediterranean Sea between Damietta sea port and Gamasa city, Egypt. Al-Azhar Bull. Sci., 28(1):1-13.

Rittmann, A. and F. M. Nakhla, 1958. Contribution to the study of Egyptian black sands. Egypt. J. Chem., 1(1):127-135.

Rozendaal, A. and C. Philander, 2000. Mineralogy of heavy mineral placers along the west coast of South Africa. In: Rammlmair D., J. Mederer, T. Oberthür, R. B. Heimann and H. Pentinghaus (Eds.), Applied Mineralogy in Research, Economy, Technology, Ecology and Culture. Proc. 6th Int. Congr. Appl. Mineral. (ICAM 2000), Göttingen, Germany, A. A. Balkema, Rotterdam, 417-420.

Samy, Y. and A. El-Gohary, 2013. Heavy minerals pattern and indices as a guide for provenance and transportation of beach sands along the Northern Sinai coast, Egypt. J. Appl. Sci. Res., 9(11):5656-5664.

Shousha, H. A., M. R. Atta, A. A. Bakhit, H. M. Diab, A. A. El Hagg and S. Dahy, 2019. Natural radioactivity assessment and the associated radiological hazards for beach sand, Baltim area, Egypt. Al-Azhar Bull. Sci., 30(1):37-47.

Surour, A. A., A. A. El-Kammar, E. H. Arafa and H. M. Korany, 2003. Dahab stream sediments, South-Eastern Sinai, Egypt: A potential source of gold, magnetite and zircon. J. Geochem. Explor., 77(1):25-43.

Van Emden, B., M. R. Thornber, J. Graham and F. J. Lincoln, 1997. The incorporation of actinides in monazite and xenotime from placer deposits in Western Australia. Can. Mineral., 35(1):95-104.

Ward, J. and R. Towner, 1985. Japan. In: ESCAP / BMR, Mineral Sands in Asia and the Pacific. Mineral Concentrations and Hydrocarbon Accumulations in the ESCAP Region, Vol. 4, UN ESCAP, Bangkok, Thailand, 76-80.

Wassef, S. N. and M. A. Mikhail, 1981. Distribution and mineralogy of ilmenite and other accessory minerals in the beach sands of west Rosetta, Egypt. Desert Inst. Bull. A.R.E., 31(1-2):17-29.

Wiegel, R. L., 2009. The Nile River Delta Coast and Alexandria Seaport, Egypt: A Brief Overview of History, Problems and Mitigation. Hydraulic Engineering Laboratory Report UCB/HEL-2009-1, University of California, Berkeley, USA, 16 p.

Zaghloul Z. M. and K. Kamel, 1965. The mineralogical and petrographical features of monazite from the black sands of Rosetta. J. Geol. U.A.R., 9(1):17-31.

Zhang W., Z. Zhu and C. Y. Cheng, 2011. A literature review of titanium metallurgical processes. Hydrometallurgy, 108(3-4):177-188.